Available online at www.sciencedirect.com
SCIENCE DIRECT®
Journal of Sound and Vibration 276 (2004) 869–897
JOURNAL OF SOUND AND VIBRATION
www.elsevier.com/locate/jsvi

Coupled vibration of partially fluid-filled cylindrical shells with ring stiffeners

Young-Wann Kim[a,*], Young-Shin Lee[b], Sung-Ho Ko[b]

[a] *Department of Mechanical Engineering, Yosu National University, San 96-1, Dunduck-Dong, Yosu, Chonnam, 550-749, South Korea*

[b] *Department of Mechanical Design Engineering, Chungnam National University, Daejeon, 305-764, South Korea*

Received 11 March 2003; accepted 6 August 2003

Abstract

A theoretical method is developed to investigate the coupled vibration characteristics of the ring-stiffened cylindrical shells partially filled with an inviscid, incompressible and irrotational fluid having a free surface. As the effect of free surface waves is taken into account in the analysis, the bulging and sloshing modes are studied. The Rayleigh–Ritz method is used to derive the frequency equation of the ring-stiffened and partially fluid-filled shells based on Love's thin shell theory. The solution for the velocity potential of fluid movement is assumed as a sum of two sets of linear combinations of suitable harmonic functions that satisfy Laplace equation and the relevant boundary conditions. The effect of fluid level, stiffener's number and position on the coupled vibration characteristics is investigated. To demonstrate the validity of present theoretical method, the published results are compared for simply supported shell and the finite element analysis is performed for unstiffened/stiffened, partially fluid-filled shells with clamped–free boundary condition.

1. Introduction

Thin-walled cylindrical shells can be seen in various kinds of industrial applications such as rocket propellant tanks in space boosters and space vehicles, liquid storage tanks for the accommodation of various kinds of liquids, or nuclear reactor vessels, and many more. When the unstiffened cylindrical shells are subjected to severe fluid pressure, it can buckle at a pressure. Also, these structures can be subjected to the external dynamic loads. These external dynamic

*Corresponding author.
E-mail address: ywkim@yosu.ac.kr (Y.-W. Kim).

0022-460X/$ - see front matter © 2003 Elsevier Ltd. All rights reserved.
doi:10.1016/j.jsv.2003.08.008

loads can cause the undesirable resonance and lead to fatigue. One method of imposing the structural efficiency of these shells is to stiffen them with ring stiffeners, spaced at suitable distances apart. Moreover one must use the dynamic characteristics on design of structure subjected to external dynamic loads because only vibration (not fatigue) could severely damage the sensitive equipments in airplanes and submarines, etc. Vibration characteristics of partially fluid-filled and stiffened cylindrical shells have been of primary importance for the design of the above-mentioned structures. Hence, numerous researches on this subject of partially fluid-filled and unstiffened shells have been conducted by different approaches such as eigenfunction expansion method [1], Galerkin's method [2], Rayleigh's quotient method [3], Rayleigh–Ritz method [4], the finite element method [5–7], the collocation method [8], the Fourier series expansion method [9] and experiment [10]. For the ring-stiffened cylindrical shell without fluid many researchers [11–14] conducted the free vibration analysis. The literature on the vibrations of partially fluid-filled and ring-stiffened cylindrical shell is less extensive. Gupta [15] considered the cylindrical shell with a ring on a free edge at top of shell. In his study, the influence of the top ring beam was estimated by changing the boundary conditions at the top of the tank from a free end to a simply supported end. Amabili et al. [4] presented the numerical results for the tank with only one stiffener.

In this paper, a theoretical method is presented for the free vibration analysis of the partially fluid-filled and ring-stiffened cylindrical shells with simply supported or clamped–free boundary condition. For the vibration of the shell itself Rayleigh–Ritz method used, it is based on Love's thin shell theory. It is assumed that the contained fluid is incompressible and inviscid. For the vibration relevant to the fluid, the solution for the velocity potential is assumed as a sum of two sets of velocity potential: one is that of the fluid associated with the flexible shell, the other is due to the sloshing of the fluid in the rigid tank. The Rayleigh–Ritz method is used to derive the frequency equation of partially fluid-filled and ring stiffened shell. To demonstrate the validity of present theoretical method, the published results are compared for simply supported shell and the finite element analysis is performed for unstiffened/stiffened, partially liquid-filled shells with clamped–free boundary condition.

2. Energy of shell and ring stiffeners

Consider the thin-walled cylindrical shell of length L, radius R and thickness h as shown in Fig. 1. The shell is stiffened evenly or unevenly by ring stiffeners with a rectangular cross-section of height d_r and width (or thickness) b_r. The kth ring stiffener is located at a distance x_k measured from one end of the shell. The stiffening technique considered in this paper is external eccentricity that stiffeners are placed outwardly to the shell middle surface. The shell and stiffeners are assumed to be made of an elastic material with Young's modulus E, the Poisson ratio v and mass density ρ. The bottom of the shell is assumed to be flat and rigid. The radial, circumferential and axial co-ordinates are denoted by r (or z), θ and x, respectively. The tank is filled to a height H with a non-viscous, incompressible and irrotational fluid of mass density ρ_L.

The considered ring stiffeners are spaced evenly or unevenly on the shell. The axial positions of stiffeners are shown in Fig. 2. The stiffeners are arranged functionally in axial direction. The

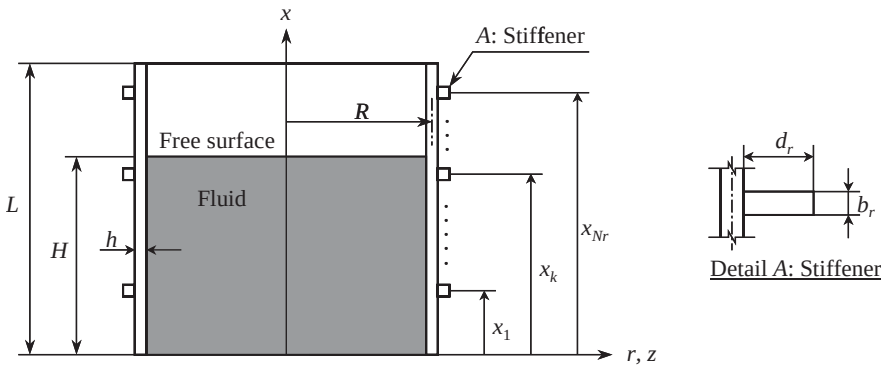

Fig. 1. Configuration of ring stiffened cylindrical shell partially filled with liquid.

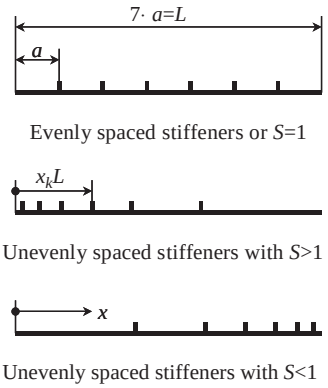

Fig. 2. Ring stiffener arrangement.

symbol x_k denoting the stiffener's position is given in terms of space ratio S:

$$x_k = \frac{L}{2}\sum_{k=1}^{N_r} S^{k-1} \Bigg/ \sum_{i=1}^{N_r} (1+S^i), \tag{2.1}$$

where N_r is the stiffener numbers. As shown in this figure, the stiffeners are located near at $x = 0$ edge in the case of $S > 1$, $x = L$ edge of the shell in the case of $S < 1$, and evenly spaced over the shell in the case of $S = 1$.

The strain energy only for the thin isotropic cylindrical shell without the stiffeners is given by

$$U_s = \frac{1}{2}\int_0^L \int_0^{2\pi} \left[A_s\left(\varepsilon_x^2 + 2\nu\varepsilon_x\varepsilon_\theta + \varepsilon_\theta^2 + \frac{1-\nu}{2}\varepsilon_{x\theta}^2\right) + D_s\left(\kappa_x^2 + 2\nu\kappa_x\kappa_\theta + \kappa_\theta^2 + \frac{1-\nu}{2}\kappa_{x\theta}^2\right)\right] \mathrm{d}x\, R\, \mathrm{d}\theta, \tag{2.2}$$

$$A_s = \frac{Eh}{1-\nu^2}, \quad D_s = \frac{Eh^3}{12(1-\nu^2)}, \tag{2.3}$$

where coefficients A_s, D_s are stretching and bending stiffness of the shell. From Love's thin shell theory, the strain and curvature ε_i, κ_i $(i = x, \theta, x\theta)$ in the middle surface are as follows:

$$\varepsilon_x = \frac{\partial u}{\partial x}, \quad \varepsilon_\theta = \frac{1}{R}\left(\frac{\partial v}{\partial \theta} + w\right), \quad \varepsilon_{x\theta} = \frac{\partial u}{R\partial \theta} + \frac{\partial v}{\partial x}, \tag{2.4}$$

$$\kappa_x = -\frac{\partial^2 w}{\partial x^2}, \quad \kappa_\phi = -\frac{1}{R^2}\left(\frac{\partial^2 w}{\partial \theta^2} - \frac{\partial v}{\partial \theta}\right), \quad \kappa_{x\phi} = -\frac{1}{R}\left(2\frac{\partial^2 w}{\partial x\ \partial \theta} - \frac{\partial v}{\partial x}\right), \tag{2.5}$$

where u, v, and w are axial, circumferential and radial displacements of the shell on the shell middle surface, respectively.

By shell deformation, the rigid motion of the ring stiffener at distance z from the shell middle surface can be expressed as

$$u_r = u - z\frac{\partial w}{\partial x}, \quad v_r = v + \frac{z}{R}\left(v - \frac{\partial w}{\partial \theta}\right), \quad w_r = w, \tag{2.6}$$

where u_r, v_r, and w_r are axial, circumferential and radial rigid displacements for the ring stiffener, respectively. The deformation of x direction for the ring stiffener u_r is negligible as the ring stiffener is analogous to a beam.

The strain energy for a ring stiffener from the discrete stiffener theory [14] is

$$U_k = \frac{1}{2}\int_0^{2\pi}\int_z \delta(x - x_k)\left[A_r\varepsilon_{\theta r}^2 + D_r\left(\kappa_{\theta\theta r}^2 + \frac{1-\nu}{2}\kappa_{x\theta r}^2\right)\right](R+z)\,\mathrm{d}\theta\,\mathrm{d}z, \tag{2.7}$$

$$\varepsilon_{\theta r} = \frac{1}{R+z}\left(\frac{\partial v_r}{\partial \theta} + w_r\right), \quad \kappa_{\theta r} = -\frac{1}{(R+z)^2}\left(\frac{\partial^2 w_r}{\partial \theta^2} - \frac{\partial v_r}{\partial \theta}\right), \quad \kappa_{x\theta r} = \frac{1}{R+z}\left(2\frac{\partial^2 w_r}{\partial x\ \partial \theta} - \frac{\partial v_r}{\partial x}\right), \tag{2.8}$$

$$A_r = \frac{Eb_r}{1-\nu^2}, \quad D_r = \frac{Eb_r^3}{12(1-\nu^2)}, \tag{2.9}$$

where subscript r means the ring stiffener and $\varepsilon_{\theta r}$, $\kappa_{\theta r}$ and $\kappa_{x\theta r}$ are circumferential strain, bending and twisting curvature of the ring stiffener in the middle surface of shell, respectively.

The kinetic energies of the shell and stiffener are given by

$$T_s = \frac{1}{2}\rho h\omega^2 \int_0^{2\pi}\int_0^L [u(x,\theta)^2 + v(x,\theta)^2 + w(x,\theta)^2]\,\mathrm{d}x\,R\,\mathrm{d}\theta, \tag{2.10}$$

$$T_k = \frac{1}{2}\rho b_r\omega^2 \int_0^{2\pi}\int_z \delta(x - x_k)\,[v_r^2(x,\theta) + w_r^2(x,\theta)](R+z)\,\mathrm{d}\theta\,\mathrm{d}z, \tag{2.11}$$

where ω is the natural angular frequency of vibration for the considered models.

In this paper, two types of boundary condition are considered: (1) SS boundary condition is both edges simply supported, (2) CF boundary condition is clamped at $x = 0$ and free at $x = L$.

The admissible displacement functions [13] for freely vibrating cylindrical shell with any boundary conditions can be written by

$$u(x,\theta)=\sum_{m=1}^{M} U_{mn}\frac{\partial\psi_m(x)}{\alpha_m\partial x}\cos n\theta,\quad v(x,\theta)=\sum_{m=1}^{M} V_{mn}\psi_m(x)\sin n\theta,$$
$$w(x,\theta)=\sum_{m=1}^{M} W_{mn}\psi_m(x)\cos n\theta, \tag{2.12}$$

where U_{mn}, V_{mn}, W_{mn} are the amplitudes for each direction, m and n are axial and circumferential wave number. $\psi_m(x)$ used as the axial mode is the beam function satisfying the described boundary condition.

3. Energy of fluid

A large number of papers on the vibrations of partially fluid-filled shells have been published, e.g., Refs. [1–10]. This formulated part is an elaboration of the theory and the approach developed by Amabili et al. in Ref. [4].

The irrotational motion of an incompressible and non-viscous fluid can be described by a velocity potential $\bar{\phi}(r,\theta,x,t)$. This potential function must satisfy the Laplace equation

$$\frac{\partial^2\bar{\phi}}{\partial r^2}+\frac{1}{r}\frac{\partial\bar{\phi}}{\partial r}+\frac{1}{r^2}\frac{\partial^2\bar{\phi}}{\partial\theta^2}+\frac{\partial^2\bar{\phi}}{\partial x^2}=0. \tag{3.1}$$

The velocity potential is assumed to be harmonic by following form

$$\bar{\phi}(r,\theta,x,t)=-\mathrm{i}\omega\phi(r,\theta,x)\mathrm{e}^{\mathrm{i}\omega t}, \tag{3.2}$$

where i is the imaginary unit and $\phi(r,\theta,x)$ is the deformation potential.

The deformation potential using the principle of superposition can be divided into

$$\phi=\phi^{(1)}+\phi^{(S)}, \tag{3.3}$$

where $\phi^{(1)}$ describes the deformation potential of the fluid associated with the flexible shell considering the bottom as rigid, $\phi^{(S)}$ describes the deformation potential due to the sloshing of the fluid in rigid tank.

Since the velocity vector of the fluid is the gradient of velocity potential, the boundary conditions imposed to the fluid are:

(a) at the rigid bottom of shell $x=0$, the fluid velocity in the vertical direction is zero, so

$$\frac{\partial\phi^{(1)}}{\partial x}=0\quad\text{at } x=0; \tag{3.4}$$

(b) the flow adjacent to the wall of the elastic shell $r=R$ must move radially with the same velocity as the shell, so

$$\frac{\partial\phi^{(1)}}{\partial r}=w(x,\theta)\quad\text{at } r=R; \tag{3.5}$$

(c) at the free surface of fluid $x = H$, the dynamic pressure is zero, so

$$\phi^{(1)} = 0 \quad \text{at } x = H. \tag{3.6}$$

The boundary conditions imposed to the deformation potential $\phi^{(S)}$ due to the sloshing of the fluid in rigid tank are:

(a) the bottom of the shell $x = 0$ is rigid the fluid velocity in the vertical direction is zero, so

$$\frac{\partial \phi^{(S)}}{\partial x} = 0 \quad \text{at } x = 0; \tag{3.7}$$

(b) the radial velocity is zero as the wall of the shell is rigid, so

$$\frac{\partial \phi^{(S)}}{\partial r} = 0 \quad \text{at } r = R; \tag{3.8}$$

(c) at the free surface $x = H$, the sloshing condition is

$$\omega^2 \phi = g \frac{\partial \phi}{\partial x} \quad \text{at } x = H, \tag{3.9}$$

where g is the gravitational acceleration. Using condition (3.6), the sloshing condition (3.9) can be rewritten as

$$\omega^2 \phi^{(S)} = g \frac{\partial}{\partial x}(\phi^{(1)} + \phi^{(S)}) \quad \text{at } x = H. \tag{3.10}$$

The kinetic energy of fluid inside the tank T_L can be written by

$$T_L = \frac{1}{2}\rho_L \omega^2 \int\int_S \phi \frac{\partial \phi}{\partial \bar{n}} \mathrm{d}S = \frac{1}{2}\rho_L \omega^2 \int\int_{S_F} \phi \frac{\partial \phi}{\partial \bar{n}} \mathrm{d}S_F + T_L^*, \tag{3.11}$$

where, $\bar{n}$ denotes the normal unit vector at any point on the boundary surface S, $S = S_1 + S_F$, S_1 is the shell lateral surface, S_F is the free surface.

When the effect of the free surface wave is neglected, the first term of second equality is zero. And the simplified kinetic energy T_L^* of the fluid is

$$\begin{aligned} T_L = T_L^* &= \frac{1}{2}\rho_L \omega^2 \int\int_{S_1} \phi \frac{\partial \phi}{\partial \bar{n}} \mathrm{d}S \\ &= \frac{1}{2}\rho_L \omega^2 \int\int_{S_1} \phi \frac{\partial \phi}{\partial r} \mathrm{d}S \\ &= \frac{1}{2}\rho_L \omega^2 \int\int_{S_1} (\phi^{(1)} + \phi^{(S)}) w \, \mathrm{d}S \\ &= T_L^{(1)} + T_L^{(1-S)}. \end{aligned} \tag{3.12}$$

The deformation potential of the fluid $\phi^{(1)}$ associated with the flexible shell considering the bottom as rigid is assumed as

$$\phi^{(1)}(x, r, \theta) = \sum_{m=1}^{M} \sum_{\bar{m}=1}^{\bar{M}} \Phi_{m\bar{m}}^{(1)} = \sum_{m=1}^{M} \sum_{\bar{m}=1}^{\bar{M}} A_{m\bar{m}n} \cos \frac{(2\bar{m}-1)\pi x}{2H} I_n\left(\frac{(2\bar{m}-1)\pi r}{2H}\right) \cos n\theta. \tag{3.13}$$

This function satisfies the boundary conditions (3.4) and (3.6) and Laplace equation (3.1). The condition given in Eq. (3.5) gives the following relation:

$$\sum_{\bar{m}=1}^{\bar{M}} A_{m\bar{m}n} \cos\frac{(2\bar{m}-1)\pi x}{2H} I'_n\left(\frac{(2\bar{m}-1)\pi R}{2H}\right) = W_{mn}\psi_m(x), \tag{3.14}$$

$$I'_n\left(\frac{(2\bar{m}-1)\pi r}{2H}\right) = \frac{(2\bar{m}-1)\pi}{4H}\left[I_{n-1}\left(\frac{(2\bar{m}-1)\pi r}{2H}\right) + I_{n+1}\left(\frac{(2\bar{m}-1)\pi r}{2H}\right)\right]. \tag{3.15}$$

This equation must be satisfied for all values $0 \leqslant x \leqslant H$. By multiplying this equation by $\cos[(2\bar{m}-1)\pi x/(2H)]$ and integrating between 0 and H, the following relation is obtained,

$$A_{m\bar{m}n} = \frac{2W_{mn}\gamma_{m\bar{m}}}{I'_n((2\bar{m}-1)\pi R/2H)H}, \quad \gamma_{m\bar{m}} = \int_0^H \psi_m(x)\cos\frac{(2\bar{m}-1)\pi x}{2H}\,\mathrm{d}x. \tag{3.16}$$

The component $\Phi^{(1)}_{m\bar{m}}$ in Eq. (3.13) can be rewritten by

$$\Phi^{(1)}_{m\bar{m}} = \sum_{\bar{m}=1}^{\bar{M}} \frac{2W_{mn}\gamma_{m\bar{m}}}{I'_n((2\bar{m}-1)\pi R/2H)H}\cos\frac{(2\bar{m}-1)\pi x}{2H} I_n\left(\frac{(2\bar{m}-1)\pi r}{2H}\right)\cos n\theta. \tag{3.17}$$

Therefore, the term $T^{(1)}_L$ in Eq. (3.12) can be written in the form

$$\begin{aligned} T^{(1)}_L &= \frac{1}{2}\rho_L\omega^2 \int_0^{2\pi}\int_0^H \phi^{(1)} w\,\mathrm{d}x\,R\,\mathrm{d}\theta\Big|_{r=R} \\ &= \frac{1}{2}\rho_L\omega^2 R C_n \sum_{m=1}^{M}\sum_{j=1}^{M} W_{mn}W_{jn}\sum_{\bar{m}=1}^{\bar{M}} \frac{2\gamma_{m\bar{m}}\gamma_{j\bar{m}}}{I'_n((2\bar{m}-1)\pi R/2H)H} I_n\left(\frac{(2\bar{m}-1)\pi R}{2H}\right), \end{aligned} \tag{3.18}$$

$$C_n = \int_0^{2\pi} \cos^2 n\theta\,\mathrm{d}\theta. \tag{3.19}$$

The deformation potential $\phi^{(S)}$ due to the sloshing of the fluid in rigid tank for the asymmetric modes ($n > 0$) can be expressed by

$$\phi^{(S)} = \sum_{k=1}^{K} B_{kn}\cosh\left(\frac{\varepsilon_{kn}x}{R}\right)J_n\left(\frac{\varepsilon_{kn}r}{R}\right)\cos n\theta. \tag{3.20}$$

This equation satisfies condition (3.7). Applying this expression to the boundary condition (3.8), the following equation is derived,

$$\frac{\mathrm{d}J_n(\varepsilon_{kn}r/R)}{\mathrm{d}r} = 0 \quad \text{at } r = R. \tag{3.21}$$

Hence ε_{kn} in Eq. (3.20) are solutions of Eq. (3.21).

Substituting expression (3.13) and (3.20) into the sloshing condition (3.10), gives

$$\omega^2 \sum_{k=1}^{K} B_{kn} \cosh\left(\frac{\varepsilon_{kn} H}{R}\right) J_n\left(\frac{\varepsilon_{kn} r}{R}\right) = -g \sum_{m=1}^{M} q_m \sum_{\bar{m}=1}^{\bar{M}} \frac{(2\bar{m}-1)\pi}{H^2} \frac{W_{mn}\gamma_{m\bar{m}}}{I_n'((2\bar{m}-1)\pi R/2H)} \sin\frac{(2\bar{m}-1)\pi}{2} I_n\left(\frac{(2\bar{m}-1)\pi r}{2H}\right) + g \sum_{k=1}^{K} B_{kn} \frac{\varepsilon_{kn}}{R} \sinh\left(\frac{\varepsilon_{kn} H}{R}\right) J_n\left(\frac{\varepsilon_{kn} r}{R}\right). \tag{3.22}$$

Eq. (3.22) must be satisfied for all range of $0 \leqslant r \leqslant R$. Multiplying this equation by $J_n(\varepsilon_{kn} r/R)r$ and integrating between 0 and R, one obtains the following sloshing equation:

$$\omega^2 \sum_{k=1}^{K} B_{kn} \cosh\left(\frac{\varepsilon_{kn} H}{R}\right) \xi_{kn} = -g \sum_{m=1}^{M} q_m \sum_{k=1}^{K} \sum_{\bar{m}=1}^{\bar{M}} \frac{(2\bar{m}-1)\pi}{H^2} \frac{W_{mn}\gamma_{m\bar{m}}}{I_n'((2\bar{m}-1)\pi R/2H)} \sin\frac{(2\bar{m}-1)\pi}{2} \zeta_{k\bar{m}n} + g \sum_{k=1}^{K} B_{kn} \frac{\varepsilon_{kn}}{R} \sinh\left(\frac{\varepsilon_{kn} H}{R}\right) \xi_{kn}, \tag{3.23}$$

$$\xi_{kn} = \int_0^R J_n^2\left(\frac{\varepsilon_{kn} r}{R}\right) r \, \mathrm{d}r, \tag{3.24}$$

$$\zeta_{k\bar{m}n} = \int_0^R J_n\left(\frac{\varepsilon_{kn} r}{R}\right) I_n\left(\frac{(2\bar{m}-1)\pi r}{2H}\right) r \, \mathrm{d}r. \tag{3.25}$$

For the axisymmetric modes ($n = 0$), $\phi^{(S)}$ can be expressed in the form

$$\phi^{(S)} = B_{00} + \sum_{k=1}^{K} B_{k0} \cosh\left(\frac{\varepsilon_{k0} x}{R}\right) J_0\left(\frac{\varepsilon_{k0} r}{R}\right). \tag{3.26}$$

The sloshing equation (3.22) is modified to the form

$$\omega^2 \left[B_{00} + \sum_{k=1}^{K} B_{k0} \cosh\left(\frac{\varepsilon_{k0} H}{R}\right) J_0\left(\frac{\varepsilon_{k0} r}{R}\right)\right] = -g \sum_{m=1}^{M} q_m \sum_{\bar{m}=1}^{\bar{M}} \frac{(2\bar{m}-1)\pi}{H^2} \frac{W_{m0}\gamma_{m\bar{m}}}{I_0'((2\bar{m}-1)\pi R/2H)} \sin\frac{(2\bar{m}-1)\pi}{2} I_0\left(\frac{(2\bar{m}-1)\pi}{2H}\right) + g \sum_{k=1}^{K} B_{k0} \frac{\varepsilon_{k0}}{R} \sinh\left(\frac{\varepsilon_{k0} H}{R}\right) J_0\left(\frac{\varepsilon_{k0} r}{R}\right). \tag{3.27}$$

Multiplying this equation by r and integrating between 0 and R, one obtains

$$\omega^2\left[B_{00}\frac{R^2}{2}+\sum_{k=1}^{K}B_{k0}\cosh\left(\frac{\varepsilon_{k0}H}{R}\right)\alpha_{k0}\right]$$
$$=-g\sum_{m=1}^{M}q_m\sum_{\bar{m}=1}^{\bar{M}}\frac{(2\bar{m}-1)\pi}{H^2}\frac{W_{m0}\gamma_{m\bar{m}}}{I_0'((2\bar{m}-1)\pi R/2H)}\sin\frac{(2\bar{m}-1)\pi}{2}\beta_{\bar{m}0}$$
$$+\ g\sum_{k=1}^{K}B_{k0}\frac{\varepsilon_{k0}}{R}\sinh\left(\frac{\varepsilon_{k0}H}{R}\right)\alpha_{k0}, \tag{3.28}$$

$$\alpha_{k0}=\int_0^R J_0\left(\frac{\varepsilon_{k0}r}{R}\right)r\,\mathrm{d}r=\frac{R^3}{\varepsilon_{k0}^2}J_1'(\varepsilon_{k0})=0, \tag{3.29}$$

$$\beta_{\bar{m}0}=\int_0^R I_0\left(\frac{(2\bar{m}-1)\pi r}{2H}\right)r\,\mathrm{d}r. \tag{3.30}$$

Eq. (3.28) can be rewritten by

$$\omega^2 B_{00}\frac{R^2}{2}=-g\sum_{m=1}^{M}q_m\sum_{\bar{m}=1}^{\bar{M}}\frac{(2\bar{m}-1)\pi}{H^2}\frac{W_{m0}\gamma_{m\bar{m}}}{I_0'((2\bar{m}-1)\pi R/2H)}\sin\frac{(2\bar{m}-1)\pi}{2}\beta_{\bar{m}0}. \tag{3.31}$$

For the asymmetric modes ($n>0$) the kinetic energy $T_L^{(1-S)}$ of the fluid due to sloshing is

$$T_L^{(1-S)}=\frac{1}{2}\rho_L\omega^2\int_0^{2\pi}\int_0^H[\phi^{(S)}w]_{r=R}\,\mathrm{d}x\,R\,\mathrm{d}\theta$$
$$=\frac{1}{2}\rho_L\omega^2 C_n R\sum_{k=1}^{K}B_{kn}J_n(\varepsilon_{kn})\sum_{m=1}^{M}W_{mn}\eta_{mkn}, \tag{3.32}$$

$$\eta_{mkn}=\int_0^H\psi_m(x)\cosh\left(\frac{\varepsilon_{kn}x}{R}\right)\mathrm{d}x. \tag{3.33}$$

For the axisymmetric modes ($n=0$) the kinetic energy $T_L^{(1-S)}$ of the fluid due to sloshing is

$$T_L^{(1-S)}=\frac{1}{2}\rho_L\omega^2 C_0 R\sum_{m=1}^{M}\left[B_{00}\tau_m+\sum_{k=1}^{K}B_{k0}J_0(\varepsilon_{k0})\eta_{mk0}\right]W_{m0}, \tag{3.34}$$

$$\tau_m=\int_0^H\psi_m(x)\,\mathrm{d}x. \tag{3.35}$$

4. Eigenvalue problem for the fluid–structure interaction

The displacement function (2.12) may be written in the matrix form

$$\{u\ \ v\ \ w\}^{\mathrm{T}}=[N_s]\{\bar{q}\},\quad \{\bar{q}\}=\{\bar{u}\ \ \bar{v}\ \ \bar{w}\}^{\mathrm{T}}, \tag{4.1}$$

where $[N_s]$ is a matrix of size $3 \times (M \times M)$ and $\{\bar{q}\}$ is a vector of the generalized co-ordinates of the shell. Vectors $\bar{u}$, $\bar{v}$, $\bar{w}$ consist of the amplitudes in displacement functions.

From Eqs. (2.2, 2.7), the strain energy of the ring stiffened elastic shell becomes

$$U_E = U_s + \sum_{k=1}^{N_r} U_k = \frac{1}{2}\{\bar{q}\}^{\mathrm{T}}[K_E]\{\bar{q}\}^{\mathrm{T}}. \tag{4.2}$$

The kinetic energy of the elastic shell from Eqs. (2.10), (2.11) expresses in matrix form

$$T_E = T_s + \sum_{k=1}^{N_r} T_k = \frac{1}{2}\omega^2\{\bar{q}\}^{\mathrm{T}}[M_E]\{\bar{q}\}. \tag{4.3}$$

In Eqs. (4.2, 4.3), matrix $[K_E]$ and $[M_E]$ are stiffness and mass matrices of elastic shells consisted of (3×3) sub-matrices as followings:

$$[K_E] = \begin{bmatrix} [K_{11}] & [K_{12}] & [K_{13}] \\ [K_{12}]^{\mathrm{T}} & [K_{22}] & [K_{23}] \\ [K_{13}]^{\mathrm{T}} & [K_{23}]^{\mathrm{T}} & [K_{33}] \end{bmatrix} \quad [M_E] = \begin{bmatrix} [M_{11}] & 0 & 0 \\ 0 & [M_{22}] & [M_{23}] \\ 0 & [M_{23}]^{\mathrm{T}} & [M_{33}] \end{bmatrix}. \tag{4.4}$$

As the cylindrical shells without/with ring stiffeners have the homogeneous geometric shape for the circumferential direction, the one term approximation is valid for the circumferential vibration mode when analyze the vibration characteristics. Hence the sizes of sub-matrices $\lfloor K_{ij} \rfloor$, $\lfloor M_{ij} \rfloor$ $(i,j = 1,2,3)$ have $(M \times M)$ dimensions and given in Appendix A.

The kinetic energy for the fluid defined in Eq. (3.12) can be written by following matrix:

$$T_L = \frac{1}{2}\omega^2\{\bar{w} \;\; \bar{B}\}\begin{bmatrix} [M_{CL}] & [M_{LS}] \\ 0 & 0 \end{bmatrix}\begin{Bmatrix} \bar{w} \\ \bar{B} \end{Bmatrix}, \tag{4.5}$$

where $[M_{CL}]$ is the added mass matrix derived from Eq. (3.18) and $[M_{LS}]$ is the added mass matrix from Eq. (3.32) for the asymmetric modes and from Eq. (3.34) for the axisymmetric modes.

For all modes, $[M_{CL}]$ with $(M \times M)$ size are

$$[M_{CL}] = \rho_L R C_n \sum_{\bar{m}=1}^{\bar{M}} \frac{2\gamma_{m\bar{m}}\gamma_{j\bar{m}}}{I_n'((2\bar{m}-1)\pi R/2H)H} I_n\left(\frac{(2\bar{m}-1)\pi R}{2H}\right) \quad \text{for } m,j = 1,\ldots,M. \tag{4.6}$$

In the case of the asymmetric modes $(n > 0)$, $[M_{LS}]$ with $(M \times K)$ size are

$$[M_{LS}] = \rho_L C_n R J_n(\varepsilon_{kn})\eta_{mkn} \quad \text{for } m = 1,\ldots,M \text{ and } k = 1,\ldots,K. \tag{4.7}$$

In the case of the axisymmetric modes $(n = 0)$, $[M_{LS}]$ is modified by adding a following additional column to Eq. (4.7) and this matrix has $(M \times (K+1))$ size.

$$[M_{LS}]_{m0} = \rho_L C_0 R \tau_m \quad \text{for } k = 0. \tag{4.8}$$

Apply the Rayleigh–Ritz method of Eq. (4.9) to find the frequency equation to investigate the vibration characteristics of the considered structures.

$$\frac{\partial}{\partial \bar{q}}[U_E - \omega^2(T_E + T_L)] = 0. \tag{4.9}$$

From Rayleigh–Ritz procedure, the following equation is obtained

$$[[K_E]\ 0]\begin{Bmatrix}\bar{q}\\ \bar{B}\end{Bmatrix} - \omega^2[[M_E + M_{CL}]\ [M_{LS}]]\begin{Bmatrix}\bar{q}\\ \bar{B}\end{Bmatrix} = 0. \tag{4.10}$$

From the sloshing equation of Eq. (3.23) or (3.31), the following matrix is obtained:

$$[[K_{CS}]\ [K_S]]\begin{Bmatrix}\bar{q}\\ \bar{B}\end{Bmatrix} - \omega^2[0\ [M_S]]\begin{Bmatrix}\bar{q}\\ \bar{B}\end{Bmatrix} = 0. \tag{4.11}$$

For the asymmetric mode,

$$[M_S] = \delta_{kk}\cosh\left(\frac{\varepsilon_{kn}H}{R}\right)\xi_{kn}, \tag{4.12}$$

$$[K_{CS}] = -g\sum_{\bar{m}=1}^{\bar{M}}\frac{(2\bar{m}-1)\pi}{H^2}\frac{W_{mn}\gamma_{m\bar{m}}}{I_n'((2\bar{m}-1)\pi R/2H)}\sin\frac{(2\bar{m}-1)\pi}{2}\zeta_{k\bar{m}n}, \tag{4.13}$$

$$[K_S] = g\delta_{kk}\frac{\varepsilon_{kn}}{R}\sinh\left(\frac{\varepsilon_{kn}H}{R}\right)\xi_{kn} \tag{4.14}$$

for $k = 1, \ldots, K$ and $m = 1, \ldots, M$. The matrices $[M_S], [K_S]$ have $(K \times K)$ and $[K_{CS}]$ has $(M \times K)$.

For the axisymmetric mode, $[M_S]$, $[K_S]$ and $[K_{CS}]$ are modified by adding the following additional row to Eqs. (4.12–4.14) and the dimensions K of these matrices must be changed into $K + 1$.

$$[M_S]_{0k} = \frac{R^2}{2g}, \tag{4.15}$$

$$[K_S]_{0k} = 0, \tag{4.16}$$

$$[K_{CS}]_{0m} = -\sum_{\bar{m}=1}^{\bar{M}}\frac{(2\bar{m}-1)\pi}{H^2}\frac{W_{m0}\gamma_{m\bar{m}}}{I_0'((2\bar{m}-1)\pi R/2H)}\sin\frac{(2\bar{m}-1)\pi}{2}\beta_{\bar{m}0} \tag{4.17}$$

for $k = 1, \ldots, K + 1$ and $m = 1, \ldots, M$.

The frequency equations of the fluid–elastic structure interface are given in Eqs. (4.19) and (4.11). These two equations can be combined into a single matrix form as

$$\begin{bmatrix}[K_E] & 0\\ [K_{CS}] & [K_S]\end{bmatrix}\begin{Bmatrix}\bar{q}\\ \bar{B}\end{Bmatrix} - \omega^2\begin{bmatrix}[M_E + M_{CL}] & [M_{LS}]\\ 0 & [M_S]\end{bmatrix}\begin{Bmatrix}\bar{q}\\ \bar{B}\end{Bmatrix} = 0. \tag{4.18}$$

The resulting eigenvalue problem can be written in the form

$$\det\left\{\begin{bmatrix}[K_E] & 0\\ [K_{CS}] & [K_S]\end{bmatrix} - \omega^2\begin{bmatrix}[M_E + M_{CL}] & [M_{LS}]\\ 0 & [M_S]\end{bmatrix}\right\} = 0. \tag{4.19}$$

For the empty shell, Eq. (4.18) reduced to following equation:

$$\det\{[K_E] - \omega^2[M_E]\} = 0. \tag{4.20}$$

Solving this eigenvalue problem the natural frequency and its corresponding mode shape are obtained.

5. Results and discussions

Some numerical examples are now demonstrated for the present theoretical method. The comparisons are made with some published data and FEM results to check the validity of the present theoretical method. ANSYS commercial FEM code [16] is used for the finite element analysis procedures. In the finite element analysis, the two-dimensional axisymmetric model is constructed with the axisymmetric structural shell element (SHELL61) for the elastic structures and fluid element (FLUID81) for the fluid region. SHELL61 has four degrees of freedom at each node: three translations in the each nodal direction and a rotation. FLUID81 is well suited for calculating fluid/solid interactions. This element is defined by four nodes having three degrees of freedom at each node: three translations in the each nodal direction. The fluid boundary conditions at the bottom of the tank are zero displacement to simulate Eq. (3.4). The radial displacements of fluid nodes along the wetted shell surfaces coincide with the corresponding displacements of the shells to present Eq. (3.5). The eigenvalue problem formulated within the FEM for the vibration analysis is solved by the reduced subspace analysis method included in the ANSYS code.

In numerical analysis, the following material properties are taken: the shell and stiffeners considered are made of a steel with: Young's modulus $E = 206$ GPa, Poisson's ratio $v = 0.3$ and mass density $\rho = 7850$ kg/m^3; the liquid is water with mass density $\rho_L = 1000$ kg/m^3.

5.1. Convergence and comparison study

To check the convergence of the present Rayleigh–Ritz method, a CF boundary conditioned shell with 4 evenly spaced ring stiffeners are analyzed. This shell is partially filled to $H/L = 0.5$ and the used dimensions are $R = 0.2$, $L = 3R$, $h = 2$ mm, $b_r = h$ and $d_r = 5b_r$. Table 1 gives the bulging natural frequencies for considered vibration modes for this shell. From the frequencies presented in this table, it may be observed that using the series terms of $M = 14$ for displacement function is adequate for converged results. The effect of the series terms K and $\bar{M}$ for the velocity potential functions is very little in the vibration results. In the analysis, the used terms are set to $K = 15$, $\bar{M} = 25$ adequately. In order to obtain the exact FEM solutions that can be used as the base line data, convergence studies were conducted for the bulging frequencies of the shell used in Table 1. The results are given in Table 2. In this table, it may be observed that the using Case 4 (fluid element number = 280, shell element number = 44) in FE analysis is adequate for the converged results.

To verify the present methodology in the presence of fluid, the published analytical and present FEA results are compared with the present theoretical results for the unstiffened/stiffened cylindrical shells partially filled with water in Tables 3 and 4. In Table 3, the analytical solutions by Kondo [1] and Amabili et al. [4] are compared with the present theoretical results for the simply supported, unstiffened cylindrical shells partially filled with water. The agreement between the results is very good and the largest discrepancy is less than 0.1% for sloshing mode, 3.0% for

Table 1
Convergence study of theoretical natural bulging frequencies (Hz) for a partially fluid-filled, ring-stiffened cylindrical shell with CF boundary condition

Mode		Number of axial series, M					
n	m	2	6	10	12	14	16
1	1	638.98	584.07	573.60	571.22	570.05	569.02
	2	1666.8	1188.7	1160.34	1154.68	1152.0	1149.9
	3	—	1740.5	1658.8	1645.8	1636.6	1634.7
2	1	297.75	286.06	282.00	281.56	281.16	280.81
	2	941.46	735.05	720.47	717.03	714.90	713.31
	3	—	1461.7	1423.1	1416.4	1410.7	1408.1
3	1	277.03	269.55	258.59	256.96	255.28	254.47
	2	594.78	508.49	498.76	496.58	494.83	494.00
	3	—	1124.6	1101.6	1097.0	1093.2	1090.9
4	1	444.38	425.56	398.21	392.99	390.05	388.31
	2	506.53	465.13	449.75	446.92	441.90	440.89
	3	—	919.09	892.70	886.92	883.11	881.41
5	1	592.26	552.82	526.07	519.66	510.44	507.66
	2	717.69	607.98	556.12	549.71	545.82	543.17
	3	—	954.09	888.12	872.44	864.57	861.88

bulging mode. The mentioned discrepancy is calculated by $(f_r - f_t)/f_r \times 100$, where f_t is the frequency of present theoretical method and f_r is that of reference or FEM. Table 4 is presented to provide additional comparison with FEM results for the clamped–free, unstiffened/stiffened cylindrical shells. The considered shell has the same dimensions used in Tables 1 and 2. For the empty shells, maximum discrepancy is less than 4.0% for the stiffened shell. In sloshing modes of partially water filled-shell, maximum discrepancy is less than 5.0% and the sloshing frequencies have the same values regardless of stiffeners. For the bulging modes, maximum discrepancy is less than 4.2% for the unstiffened shell, 4.5% for the stiffened shell. From these results shown in Tables 3 and 4, sufficient accuracy of the present theoretical method is noted. This agreement demonstrates the accuracy of the present methodology.

5.2. Natural frequencies

In order to estimate the effect of the amount of fluid on the natural frequencies of bulging modes for the fluid-filled cylindrical shell, a normalized natural frequency is defined by f_w/f_e, where f_e and f_w stand for the natural frequencies of the empty and the fluid-filled shell. The results are given in Figs. 3–8. The shells have a dimensions of $R = 0.2$ m, $L = 3R$, $h = 2$ mm, $b_r = h$, $d_r = 5b_r$.

The variation of natural frequencies for the unstiffened and stiffened shells with SS boundary condition shows in Figs. 3–5. Generally, the frequencies in lower circumferential wave number are

Table 2
Convergence study of FEM's natural bulging frequencies (Hz) for a partially fluid-filled, ring-stiffened cylindrical shell with CF boundary condition

Mode		Number of elements				
n	m	Case 1 Fluid = 40 Shell = 14	Case 2 Fluid = 100 Shell = 24	Case 3 Fluid = 180 Shell = 34	Case 4 Fluid = 280 Shell = 44	Case 5 Fluid = 400 Shell = 54
1	1	560.93	560.62	560.81	560.96	561.07
	2	1154.5	1133.8	1130.6	1129.8	1129.5
	3	1641.9	1565.8	1546.5	1539.8	1536.7
2	1	275.84	275.84	275.99	276.09	276.15
	2	703.25	695.48	694.21	693.82	693.65
	3	1428.7	1382.4	1372.4	1369.1	1367.7
3	1	249.36	246.27	245.90	245.89	245.92
	2	487.15	482.37	481.75	481.62	481.59
	3	1092.2	1063.3	1058.5	1057.1	1056.5
4	1	382.99	374.55	373.42	373.30	373.32
	2	432.52	425.13	424.17	424.00	423.98
	3	873.68	852.03	848.94	848.19	847.98
5	1	506.57	492.48	490.63	490.36	490.35
	2	545.39	530.64	528.67	528.32	528.25
	3	861.29	844.89	832.31	831.64	830.55

Table 3
Comparison study of angular frequencies (rad/s) of sloshing and bulging modes for the simply supported cylindrical shell partially fluid-filled with water ($R = 25$ m, $L = 30$ m, $H = 21.6$ m, $h = 0.03$ m)

Mode		Sloshing mode			Bulging mode		
		Amabili [4]	Kondo [1]	Present	Amabili [4]	Kondo [1]	Present
$n = 0$	1	1.2244	1.2238	1.2244	22.244	22.096	22.190
	2	1.6591	1.6582	1.6591	44.010	43.762	43.884
	3	1.9980	1.9969	1.9979	57.191	56.829	56.960
	4	2.2865	2.2853	2.2865	67.291	66.888	66.980
	5	2.5422	2.5409	2.5422	75.850	75.347	75.449
$n = 4$	1	1.4425	—	1.4426	13.658	—	14.054
	2	1.9081	—	1.9081	34.441	—	34.672
	3	2.2305	—	2.2305	49.692	—	49.629
	4	2.5027	—	2.5027	61.877	—	61.556
	5	2.7444	—	2.7444	71.804	—	71.476

Table 4
Comparison study of natural frequencies (Hz) of sloshing and bulging modes for the partially fluid-filled, unstiffened/stiffened cylindrical shells with CF boundary condition

Mode	Empty shell		Water-filled shell			
	FEM	Theory	Sloshing		Bulging	
			FEM	Theory	FEM	Theory
(a) *Unstiffened shell*						
1st	183.70(1, 3)	183.95(1, 3)	1.4356(1, 1)	1.5065(1, 1)	169.39(1, 3)	170.34(1, 3)
2nd	204.59(1, 4)	204.73(1, 4)	1.8932(1, 2)	1.9478(1, 2)	189.91(1, 4)	190.91(1, 4)
3rd	299.11(1, 5)	299.25(1, 5)	2.1416(1, 0)	2.1819(1, 0)	265.61(1, 5)	268.82(1, 5)
4th	306.50(1, 2)	307.14(1, 2)	2.2294(1, 3)	2.2847(1, 3)	272.27(1, 2)	274.98(1, 2)
5th	430.08(1, 6)	430.23(1, 6)	2.4555(2, 1)	2.5104(2, 1)	336.80(1, 6)	344.09(1, 6)
(b) *Stiffened shell*						
1st	274.94(1, 3)	280.23(1, 3)	1.4356(1, 1)	1.5065(1, 1)	245.89(1, 3)	255.28(1, 3)
2nd	308.72(1, 2)	312.15(1, 2)	1.8932(1, 2)	1.9478(1, 2)	276.09(1, 2)	281.16(1, 2)
3rd	408.73(1, 4)	419.49(1, 4)	2.1416(0, 0)	2.1819(0, 0)	373.30(1, 4)	390.05(1, 4)
4th	538.47(1, 5)	551.46(1, 5)	2.2294(1, 3)	2.2847(1, 3)	424.00(2, 4)	441.90(2, 4)
5th	626.39(1, 6)	652.40(1, 6)	2.4555(2, 1)	2.5104(2, 1)	481.62(2, 3)	494.83(2, 3)

Numbers in (m, n) of empty and bulging modes represent the axial and circumferential wave number. Numbers in (k, n) of sloshing modes represent the nodal circle and diameter number of free surface.

much more decreased than those in higher circumferential wave number with the increase of the fluid-filling ratio (or fluid level) except for some mode of each shell. In the case of the first axial mode ($m = 1$), the frequency variations for the considered shells are very similar except for $n > 5$ modes. The effect of fluid level in the range of $0.1 < H/L < 0.5$ is very large for $n > 5$ mode but for the stiffened shells with unevenly spacing of $S = 2$. In this range the effect of fluid level for the stiffened shells with unevenly spacing of $S = 2$ is very small for $n > 5$ modes. The frequency variations are different from each other axial wave number. The natural frequencies of a fully fluid-filled cylindrical shell were decreased about 60% corresponding to those of the empty shell. The normalized frequencies do not linearly vary according to fluid level. The variation of natural frequencies for the unstiffened and stiffened shell with CF boundary condition shows in Figs. 6–8. The effect of fluid level for CF boundary conditioned shell is less than that for SS boundary conditioned shell in small fluid levels. For the $m = 1$ mode, the effect of fluid level is very small in small filling ratio ($H/L < 0.4$). As shown in figures, the frequency variation with fluid level is very different among the stiffening methods and the effect of stiffening method is very large. The general behavior with the filling ratio is similar to SS boundary conditioned shells. It is notable that there are some fluid-filled regions that normalized frequencies are almost same. This means that the frequencies in these filling ratios are almost same regardless of fluid level. This does not mean that the hydrodynamic mass due to fluid motion increases always with increase of fluid level. Generally, the normalized frequency decreases to the minimum value of a fully fluid-filled shell due to the increase of hydrodynamic mass induced by the fluid motion during vibration as the amount of fluid increases. The variation of the normalized frequency for the fluid filled-shell depends on the axial and circumferential wave number.

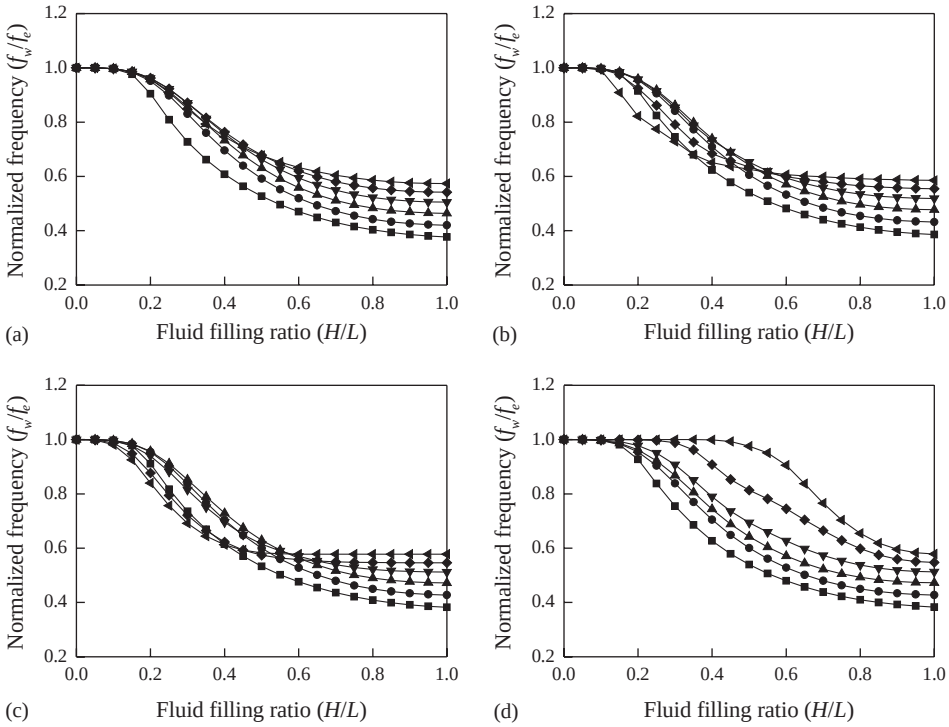

Fig. 3. Effect of fluid level on frequencies of the first axial bulging mode ($m = 1$) for unstiffened and 4-externally eccentric ring stiffened shell with SS boundary condition: (a) unstiffened shell; (b) stiffened shell with evenly spacing; (c) stiffened shell with unevenly spacing of $S = 0.5$; (d) stiffened shell with unevenly spacing of $S = 2.0$: ■, $n = 1$; ●, $n = 2$; ▲, $n = 3$; ▼, $n = 4$; ◆, $n = 5$; ◀, $n = 6$.

Fig. 9 shows the first three normalized sloshing frequency variations with nodal diameters for the shell of $R = 0.2$ m, $L = 3R$, $h = 2$ mm. The normalized frequency is defined by f_p/f_f, where f_p and f_f stand for the natural frequencies of the partially and the fully fluid-filled shell. The sloshing frequencies of the shells with the same R and L are almost same regardless of boundary conditions and ring stiffening (see Table 4). We can explain this phenomenon that the deformation of shell does not occur in the sloshing vibration mode. The shell deformation does not occur because the shell is stiff enough for sloshing but an extremely flexible shell will show larger displacement. The sloshing frequencies first increase dramatically as the fluid level increases and then remain almost constant regardless of any increase of fluid level. The frequency of first mode for $n = 1$ first increase up to $H/L = 0.4$. The frequency of the other mode increase up to $H/L = 0.1$–0.2. The effect of fluid level on sloshing frequency becomes small for higher nodal circle vibration mode. Therefore, it is sufficient to consider fluid level up to 40% of shell length for the sloshing frequency analysis of fluid in storage tank.

Figs. 10 and 11 give to investigate the effect of number of stiffener on the fundamental frequency of bulging mode for evenly or unevenly spaced, stiffened shell with CF and SS boundary conditioned shells of $R = 0.4$ m, $L = 4R$, $h = 2$ mm, $b_r = 2h$, $d_r = 3b_r$. In the figure, change of fundamental frequency calculated by $(f_s - f_u)/f_u \times 100$, where f_u, f_s stand for the

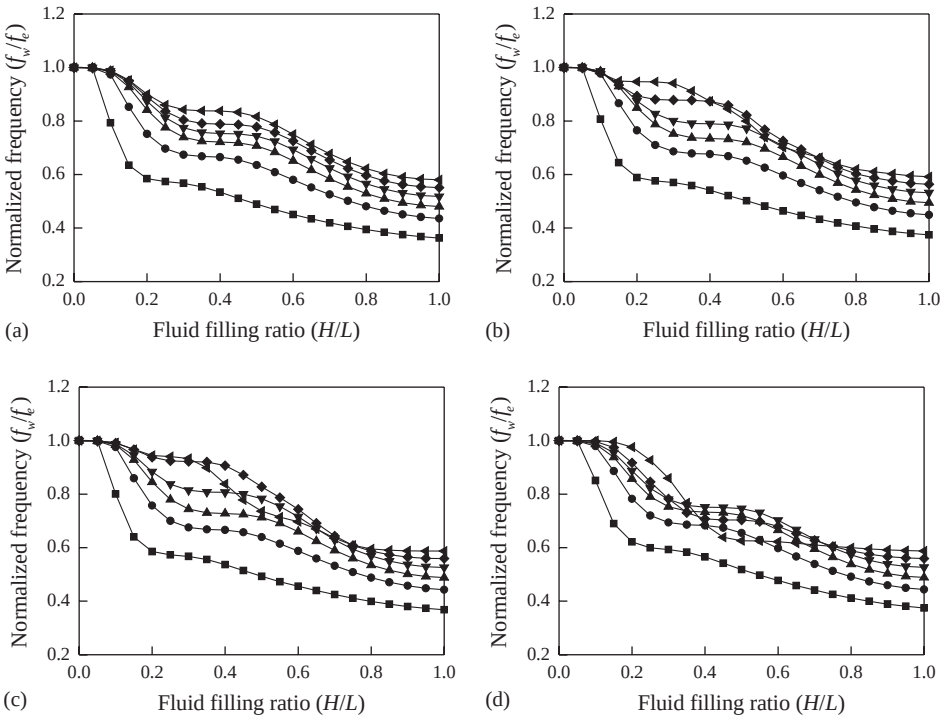

Fig. 4. Effect of fluid level on frequencies of the second axial bulging mode ($m = 2$) for unstiffened and four-externally eccentric ring stiffened shell with SS boundary condition: (a) unstiffened shell; (b) stiffened shell with evenly spacing; (c) stiffened shell with unevenly spacing of $S = 0.5$; (d) stiffened shell with unevenly spacing of $S = 2.0$: ■, $n = 1$; ●, $n = 2$; ▲, $n = 3$; ▼, $n = 4$; ◆, $n = 5$; ◀, $n = 6$.

fundamental frequencies of the unstiffened and stiffened shell. As shown in Fig. 10 for the CF boundary conditioned shell, the frequencies first increase rapidly and then smoothly for the stiffened shells with evenly spacing and unevenly spacing of $S = 1/1.75$ as the number of stiffener increase. However for the stiffened shell with unevenly spacing of $S = 1/1.75$ which are partially filled to $H/L = 0.25$ by fluid and the empty shell, the frequencies decrease with increasing the stiffener number in the case of stiffening by a large number of stiffener. The reason of frequency decreasing is that the stiffness effect is smaller than mass effect by increase of ring stiffener number. For the stiffened shell with unevenly spacing of $S = 1.75$, the frequencies first increase smoothly and then remain constant with the increase of ring stiffener number. The behavior of frequency variation for the empty shell and the fluid-filled shell up to $H/L = 0.25$ is almost same. The frequency increment by ring stiffening is the largest for the stiffened shell with evenly spacing, the smallest for the stiffened shell with unevenly spacing of $S = 1.75$. The maximum increment is about 85% for the stiffened shell with evenly spacing, 80% for the stiffened shell with unevenly spacing with $S = 1/1.75$ and 22% for the stiffened shell with unevenly spacing of $S = 1.75$. The effect of stiffener is the largest for the unevenly spaced shell of $S = 1/1.75$ in the case of stiffening by small number of stiffener. The effect of stiffener for the partially fluid-filled shell decreases with increase of fluid amount. For the SS boundary conditioned shell, the frequency variation with

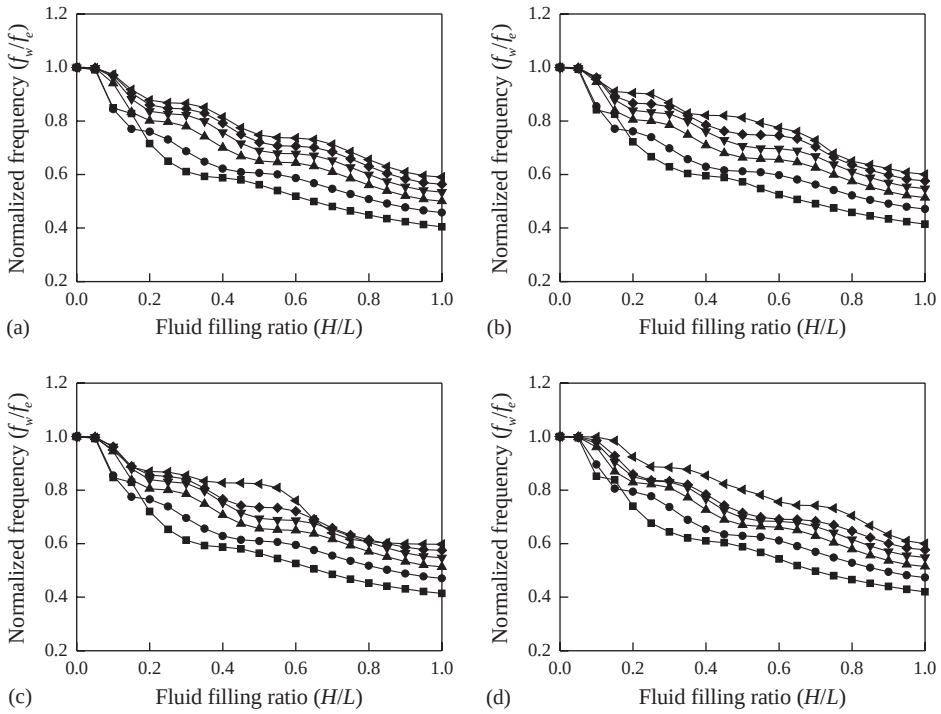

Fig. 5. Effect of fluid level on frequencies of the third axial bulging mode ($m = 3$) for unstiffened and four-externally eccentric ring stiffened shell with SS boundary condition: (a) unstiffened shell; (b) stiffened shell with evenly spacing; (c) stiffened shell with unevenly spacing of $S = 0.5$; (d) stiffened shell with unevenly spacing of $S = 2.0$: ■, $n = 1$; ●, $n = 2$; ▲, $n = 3$; ▼, $n = 4$; ◆, $n = 5$; ◀, $n = 6$.

stiffener number is shown in Fig. 11. Unlike the CF boundary conditioned shell, there is the frequency gap between the empty and small amount fluid-filled shell. This reason can be explained that the effect of filling ratio is greater than for the CF boundary conditioned shell in small fluid level as indicated in Fig. 3. For two types of the unevenly spaced shells, frequency variation is almost same. By ring stiffening, the frequency increases up to 75% for the stiffened shell with evenly spacing and 60% for the shell of unevenly spacing. The general behavior is similar to CF boundary conditioned shell.

From two figures, the stiffening method by evenly spacing or unevenly spacing of $S<1$ for the CF boundary conditioned shell is more influenced on the fundamental frequency than by unevenly spacing of $S > 1$. This means that it is more effective to locate the ring at free edge for the CF boundary conditioned shell when the shell is stiffened unevenly by ring stiffeners to increase the fundamental frequency. But for the SS boundary conditioned shell, the evenly spacing of ring stiffeners is more effective than unevenly spacing. The effect of stiffener for the CF boundary conditioned shell is greater than for the SS boundary conditioned shell.

Figs. 12 and 13 show the fundamental frequency variation with spacing ratio or stiffener position. Fig. 12 indicates the frequency variation with stiffener position for the one-ring stiffened shell. The dimensions of shell used in Fig. 12 are $R = 0.4$ m, $L = 2R$, $h = 2$ mm, $b_r = 5h$ and $d_r = 2b_r$. For the CF boundary conditioned shell the fundamental frequencies increase as the

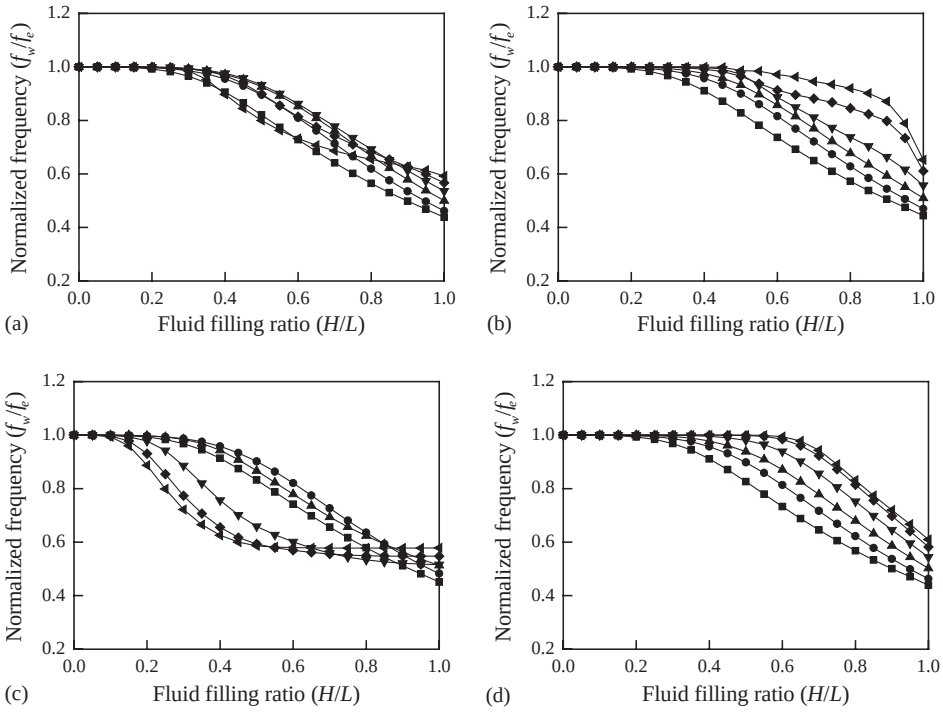

Fig. 6. Effect of fluid level on frequencies of the first axial bulging mode ($m = 1$) for unstiffened and four-externally eccentric ring stiffened shell with CF boundary condition: (a) unstiffened shell; (b) stiffened shell with evenly spacing; (c) stiffened shell with unevenly spacing of $S = 0.5$; (d) stiffened shell with unevenly spacing of $S = 2.0$: ■, $n = 1$; ●, $n = 2$; ▲, $n = 3$; ▼, $n = 4$; ◆, $n = 5$; ◀, $n = 6$.

stiffener position is near to free edge. But the frequencies decrease in case that stiffener is positioned to free edge exactly. It is more efficient stiffening method that the stiffener is located near to free edge ($0.9 < x/L < 1$) to increase the fundamental frequency for the shells with CF boundary condition. By stiffening the shell with only one stiffener, the frequencies increase to 90–120% according to fluid level compared with the unstiffened shell. For the SS boundary conditioned shell, as the stiffener is located near to the center of shell the frequencies increase. The optimal position is $x/L = 0.4$ for the partially fluid-filled shell up to $H/L = 0.25$, 0.5 and $x/L = 0.5$ for the other shells to have maximum frequency. By stiffening the shell with only one stiffener, the frequencies increase to 80–150% according to fluid level compared with the unstiffened shell. Fig. 13 shows the frequency variation with stiffener position for the five-ring stiffened shell. The shells have a dimension of $R = 0.4$ m, $L = 2R$ and the ring stiffeners have $b_r = 2h$, $d_r = 4b_r$. In the case of the CF boundary conditioned shell, the frequency is larger for the stiffened shells with unevenly spacing of $S < 1$ but smaller for the stiffened shells with unevenly spacing of $S > 1$ than that of the stiffened shells with evenly spacing. The frequencies increase gradually and then decrease as the spacing ratio become small, that is, stiffeners is positioned from the near clamped edge to the near free edge. In the case of SS boundary conditioned shell, the frequencies gradually decrease as the stiffener spacing ratio (S) becomes small or large. This means that the frequencies

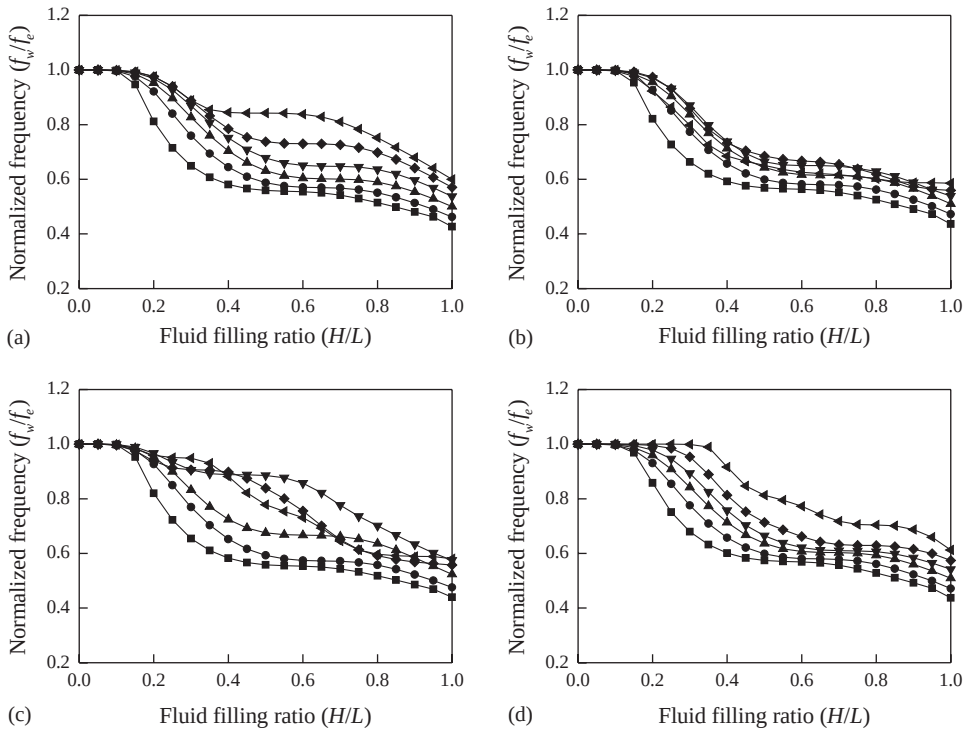

Fig. 7. Effect of fluid level on frequencies of the second axial bulging mode ($m = 2$) for unstiffened and four-externally eccentric ring stiffened shell with CF boundary condition: (a) unstiffened shell; (b) stiffened shell with evenly spacing; (c) stiffened shell with unevenly spacing of $S = 0.5$; (d) stiffened shell with unevenly spacing of $S = 2.0$: ■, $n = 1$; ●, $n = 2$; ▲, $n = 3$; ▼, $n = 4$; ◆, $n = 5$; ◀, $n = 6$.

decrease as the stiffeners are positioned to a boundary edge of shell. The frequencies for the partially fluid-filled shell are the smallest in case that the stiffeners locate to empty region, i.e., $S = 0.5$. The stiffened shells with unevenly spacing of $S = 1.25$ have the largest frequencies. The results show that the frequency may be significantly influenced by the stiffener position. Designers may obtain the desirable frequency suitable to design purpose as the stiffeners are arranged appropriately. From Figs. 12 and 13, the effect of fluid level on the fundamental frequency of SS boundary conditioned shell is larger than that of CF shell.

5.3. Vibration mode shapes

To see the variation of the axial vibration mode shape with fluid level, stiffener position and circumferential wave number, axial vibration mode shapes are plotted in Figs. 14–17.

To show the effect of the fluid level and stiffener position on the axial mode shapes, variations of mode shape for $n = 5$ are plotted in Fig. 14 for the one-ring stiffened shell with CF boundary condition. The effect of stiffener position is very great on mode shapes. As shown in the figures, the stiffener restrains the deformation of shell. The effect of fluid level on the first mode is large for stiffened shell at $x/L = 0.75$ and very small for the unstiffened shell and stiffened shells at

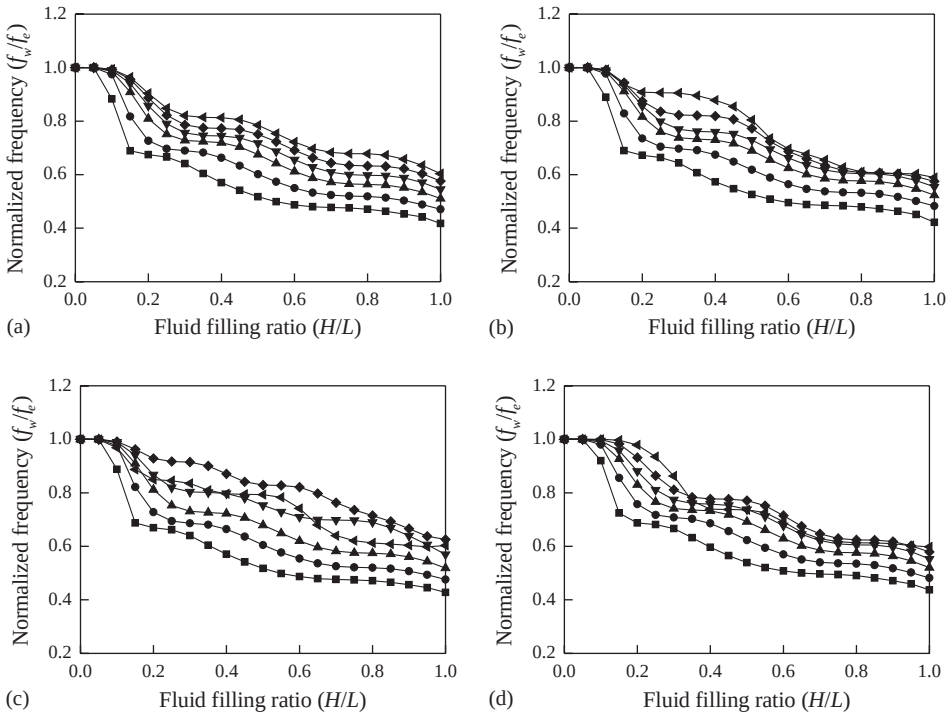

Fig. 8. Effect of fluid level on frequencies of the third axial bulging mode ($m = 3$) for unstiffened and four-externally eccentric ring stiffened shell with CF boundary condition: (a) unstiffened shell; (b) stiffened shell with evenly spacing; (c) stiffened shell with unevenly spacing of $S = 0.5$; (d) stiffened shell with unevenly spacing of $S = 2.0$: ■, $n = 1$; ●, $n = 2$; ▲, $n = 3$; ▼, $n = 4$; ◆, $n = 5$; ◀, $n = 6$.

$x/L = 0.25$, 0.5. The fluid effect on the other modes is some large. As shown in the figures, the adding fluid changes the nodal points. For the partially fluid-filled shells up to $H/L = 0.25$–0.75 of stiffened shells at $x/L = 0.75$, the first and second mode shapes are very different to other shell. It looks like that these two mode shapes are exchanged with each other by fluid as compared to other shells.

For the one-ring stiffened shell with SS boundary condition, variations of mode shape for $n = 7$ are plotted in Fig. 15. For the unstiffened and empty shell, the mode shapes are symmetric (or antisymmetric) to center on shell but they are changed to un-symmetric by adding the fluid or the stiffener. The mode shapes of fully fluid-filled shell are similar to those of empty shell. The mode shapes of stiffened shells are very different to unstiffened shell by the effect of ring stiffener. The deformation of ring stiffening region is very small, because the dimensions of stiffener (the stiffness of stiffener) is large. Considering the small stiffener, the deformation may depend on shell modes. The second and third axial mode shapes of ring stiffened shells at $x/L = 0.25$ and 0.75 are influenced by fluid level but the first mode shapes are not. The effect of fluid is great for the stiffened shell with a ring at $x/L = 0.5$. For the empty and fully fluid-filled shells with a ring stiffener at $x/L = 0.5$ the first and second mode shapes are exchanged compared to those of unstiffened shell. For the partially fluid-filled shell the first and second mode shapes have reversed

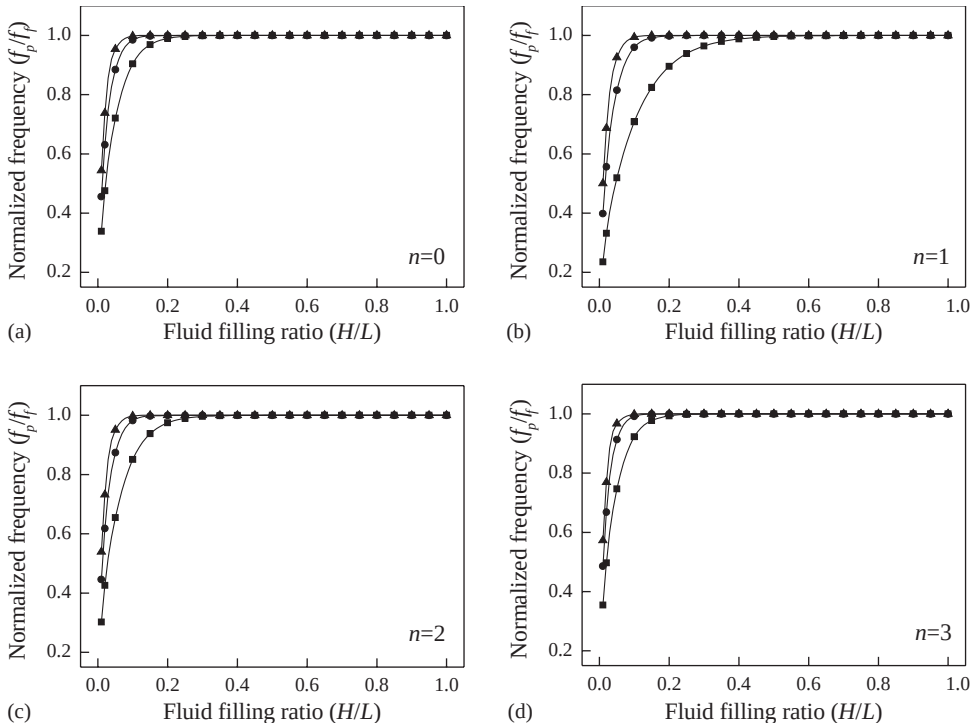

Fig. 9. Natural frequency of the first three sloshing mode for each nodal diameter (n): ■, first mode; ●, second mode; ▲, third mode.

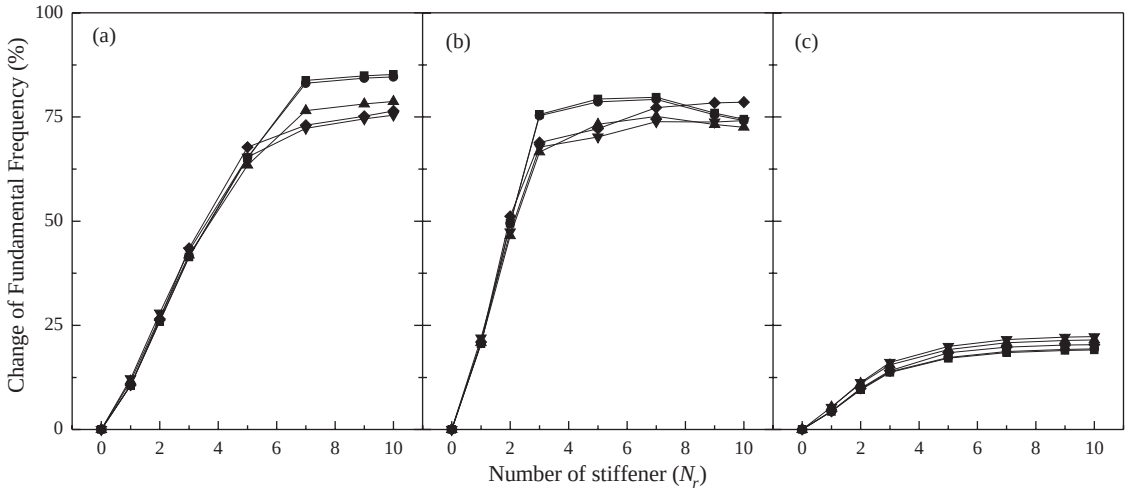

Fig. 10. Effect of number of stiffener on frequency of bulging mode for stiffened shell with CF boundary condition: ■, $H/L = 0$; ●, $H/L = 0.25$; ▲, $H/L = 0.5$; ▼, $H/L = 0.75$; ◆, $H/L = 1$. (a) Evenly spaced shell; (b) unevenly spaced shell with $S = 1/1.75$; (c) unevenly spaced shell with $S = 1.75$.

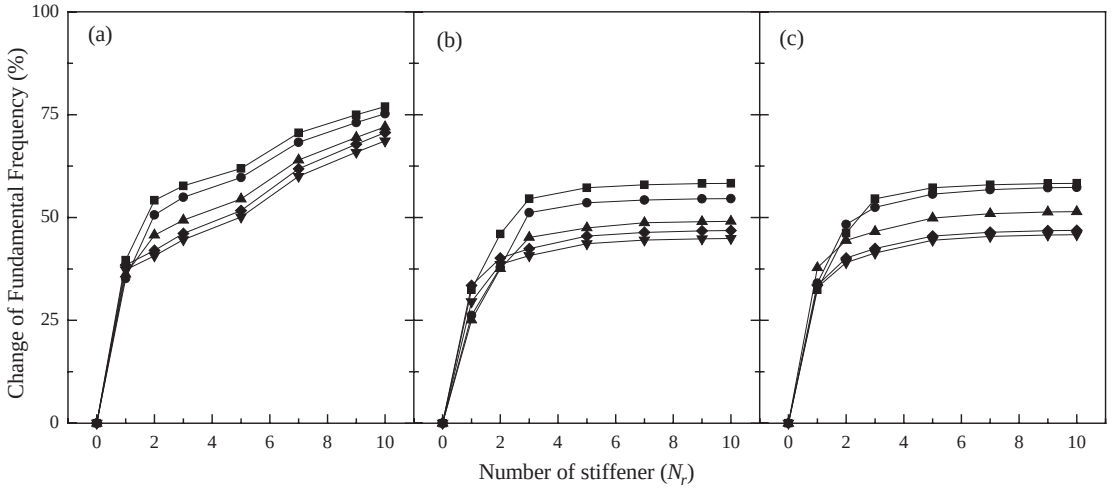

Fig. 11. Effect of number of stiffener on frequency of bulging mode for stiffened shell with SS boundary condition: ■, $H/L = 0$; ●, $H/L = 0.25$; ▲, $H/L = 0.5$; ▼, $H/L = 0.75$; ◆, $H/L = 1$. (a) Evenly spaced shell; (b) unevenly spaced shell with $S = 1/1.75$; (c) unevenly spaced shell with $S = 1.75$.

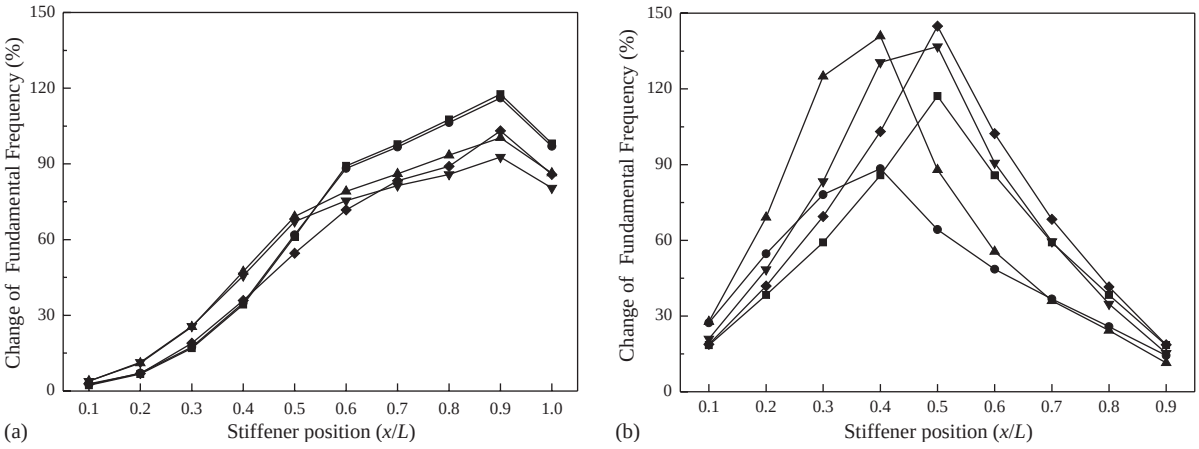

Fig. 12. Effect of position of stiffener on frequency of bulging mode for one-ring stiffened shell: ■, $H/L = 0$; ●, $H/L = 0.25$; ▲, $H/L = 0.5$; ◆, $H/L = 0.75$; ◆, $H/L = 1$. (a) CF boundary condition; (b) SS boundary condition.

shapes. The effect of stiffener on mode shapes is greater than that of fluid. The effect of fluid on mode shapes depends on stiffener position.

Fig. 16 indicates the variations of first three axial mode shapes for $n = 5$ of the five-ring stiffened shells with CF boundary condition used in Fig. 13. The mode shapes of the stiffened shells with evenly spaced rings are similar to unstiffened shell except for the partially fluid-filled shell up to $H/L = 0.5$ and 0.75. There is only local deformation by stiffeners for these shells. The mode shapes of the partially fluid-filled shell up to $H/L = 0.5$ and 0.75 are very different to other mode shapes due to fluid. The effect of fluid is very small for the partially fluid-filled shell up to

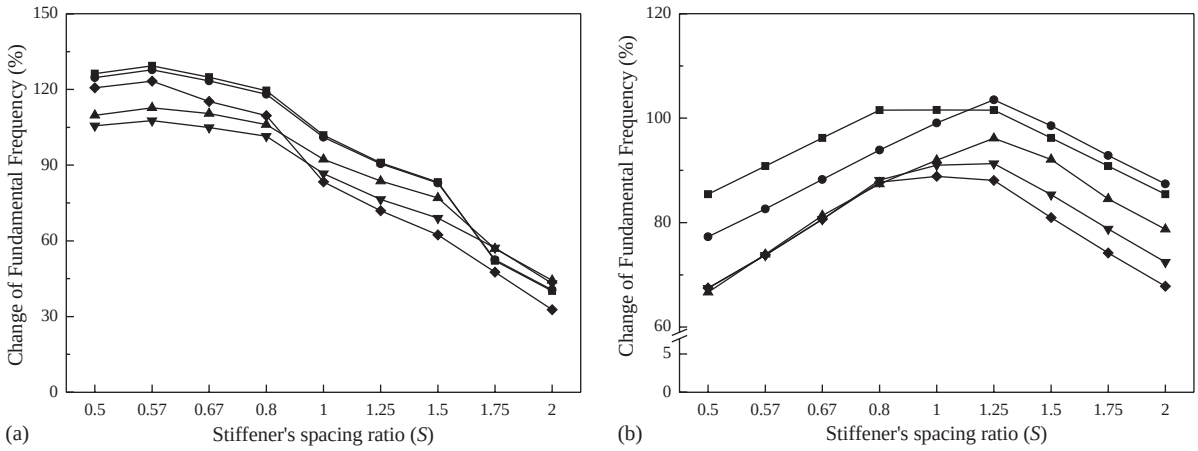

Fig. 13. Effect of position of stiffener on frequency of bulging mode for five-ring stiffened shells: ■, $H/L = 0$; ●, $H/L = 0.25$; ▲, $H/L = 0.5$; ▼, $H/L = 0.75$; ◆, $H/L = 1$. (a) CF boundary condition; (b) SS boundary condition.

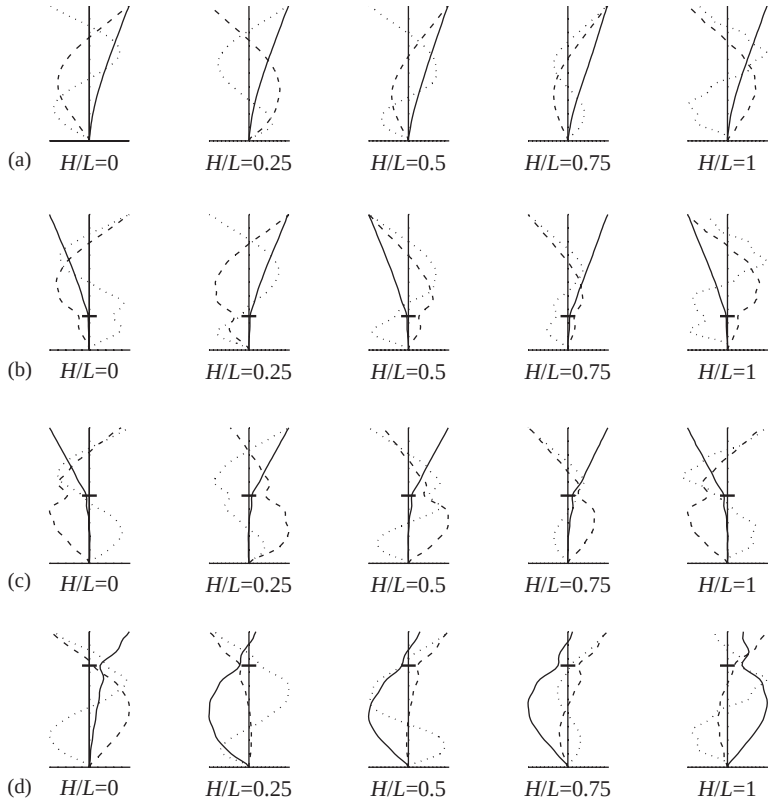

Fig. 14. Effect of stiffener position and fluid level on axial vibration mode shape for $n = 5$ of one-ring stiffened cylindrical shell with CF boundary condition used in Fig. 12: ——, position of the stiffener; —, $m = 1$; – – –, $m = 2$; - - - -, $m = 3$. (a) Unstiffened shell; (b) stiffened shell at $x_1/L = 0.25$; (c) stiffened shell at $x_1/L = 0.5$; (d) stiffened shell at $x_1/L = 0.75$.

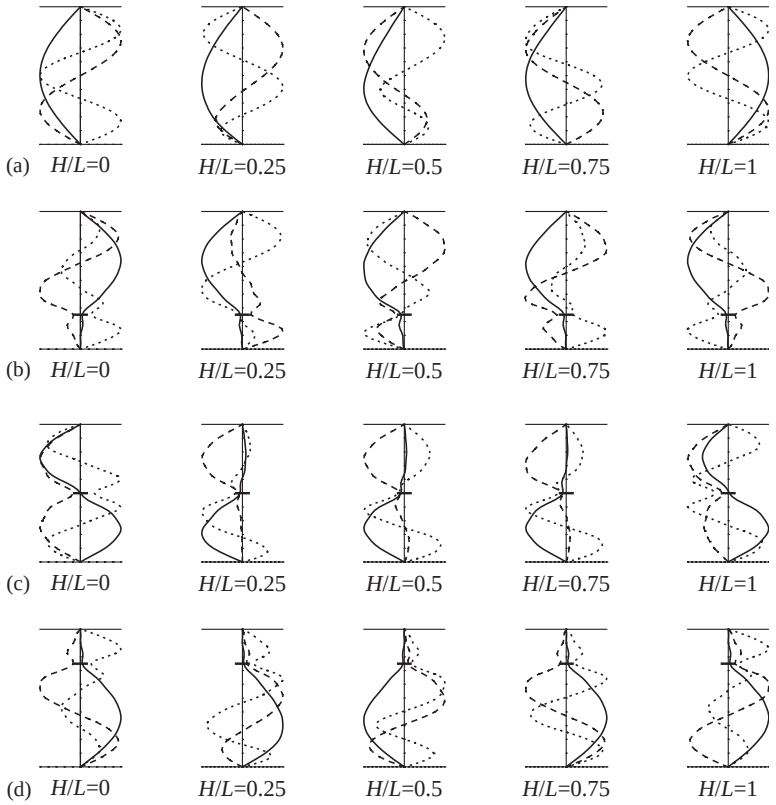

Fig. 15. Effect of stiffener position and fluid level on axial vibration mode shape for $n = 7$ of one-ring stiffened cylindrical shell with SS boundary condition used in Fig. 12: ——, position of the stiffener; —, $m = 1$; – – –, $m = 2$; - - - -, $m = 3$. (a) Unstiffened shell; (b) stiffened shell at $x_1/L = 0.25$; (c) stiffened shell at $x_1/L = 0.5$; (d) stiffened shell at $x_1/L = 0.75$.

$H/L = 0.25$ but very large for the partially fluid-filled shell up to $H/L = 0.5$ and 0.75. The effect of ring stiffener is very great for the stiffened shell with unevenly spacing, $S = 0.5$. There is no deformation at free edge for the first mode shapes by stiffeners. The mode shapes of stiffened shells with unevenly spacing, $S = 2$, are similar to those of unstiffened shells. This behavior results from that the stiffeners positioned mainly near to clamped edge.

Fig. 17 is for the SS boundary conditioned shells. The behavior of mode shapes of stiffened shells with evenly spacing is similar to unstiffened shell except for local modes by stiffeners. The effect of fluid for stiffened shells is larger than that of unstiffened shell. The effect of fluid is largest for the partially fluid-filled shells up to $H/L = 0.5$. The stiffener position makes the mode shapes different.

6. Conclusion

The theoretical method has been proposed to investigate the coupled vibration characteristics of the partially fluid-filled and ring-stiffened cylindrical shells with clamped–free or simply

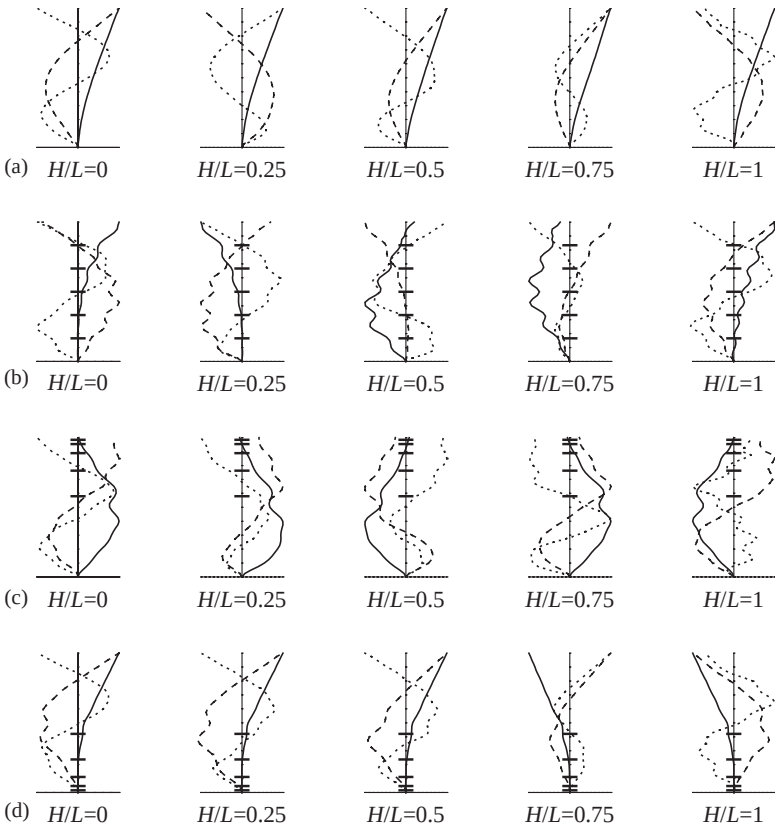

Fig. 16. Effect of stiffener position and fluid level on axial vibration mode shape for $n = 5$ of five-ring stiffened cylindrical shell with CF boundary condition used in Fig. 13: ——, position of the stiffener; —, $m = 1$; – – –, $m = 2$; - - - -, $m = 3$. (a) Unstiffened shell; (b) stiffened shell with $S = 1.0$; (c) stiffened shell with $S = 0.5$; (d) stiffened shell with $S = 2.0$.

supported boundary condition using Rayleigh–Ritz procedure. The present theoretical results are verified by comparing the present finite element analysis results from ANSYS. Based on the some numerical results, the followings are concluded.

The frequencies of bulging and sloshing mode are influenced by fluid level, that is, the frequency of bulging decreases and that of sloshing mode increases as the fluid level increases. The effect of fluid level varies with the wave number, i.e., this effect becomes large for the high wave number on bulging mode and small for the high nodal circle number on sloshing mode. The sloshing frequencies of the partially fluid-filled shells with the same dimension are almost same regardless of boundary conditions and ring stiffening. Few stiffeners are adequate for the stiffening of the cylindrical shell, and many stiffeners may decrease the frequency on the contrary. The proper arrangement of ring stiffeners may result in the desirable effect of raising the frequency. Therefore optimum (or best) design should be conducted for more efficient usages of stiffeners in the stiffened shell design. The mode shapes vary as stiffener positions and fluid level change. The effect of fluid on mode shapes depends on stiffener position. The effect of stiffener on mode shapes is greater than that of fluid.

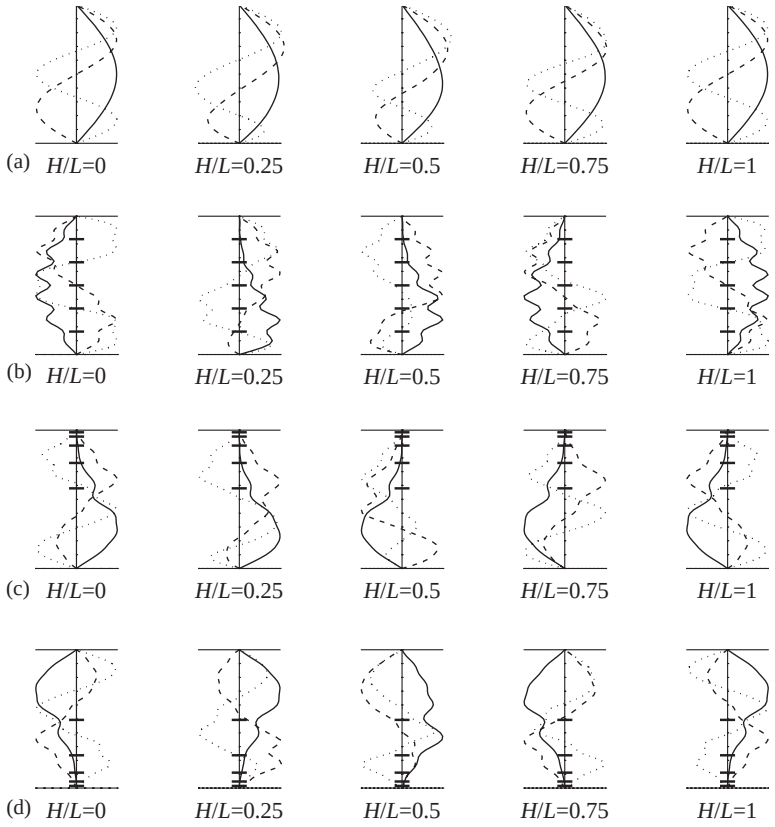

Fig. 17. Effect of stiffener position and fluid level on axial vibration mode shape for $n = 6$ of five-ring stiffened cylindrical shell with SS boundary condition used in Fig. 13: ——, position of the stiffener; —, $m = 1$; – – –, $m = 2$; - - - -, $m = 3$. (a) Unstiffened shell; (b) stiffened shell with $S = 1.0$; (c) stiffened shell with $S = 0.5$; (d) stiffened shell with $S = 2.0$.

Acknowledgements

This work was supported by Korean Research Foundation Grant (KRF-2000-E00006).

Appendix A

The sub-matrices, $\lfloor K_{ij} \rfloor$ and $\lfloor M_{ij} \rfloor$ in Equation (4.4) are as follows:

$$[K_{11}]_{m\bar{n}} = RA_s\left(\frac{X^{22}_{\bar{m}m}C_n}{\alpha_{\bar{n}}\alpha_m} + \frac{(1-\nu)n^2}{2R^2}\frac{X^{11}_{\bar{m}m}S_n}{\alpha_{\bar{n}}\alpha_m}\right), \tag{A.1}$$

$$[K_{12}]_{m\bar{n}} = nA_s\left(\frac{\nu X^{02}_{\bar{m}m}C_n}{\alpha_{\bar{n}}} - \frac{1-\nu}{2}\frac{X^{11}_{\bar{m}m}S_n}{\alpha_{\bar{n}}}\right), \tag{A.2}$$

$$[K_{c13}]_{m\bar{n}} = nvA_s \frac{X^{02}_{\bar{n}m} C_n}{\alpha_{\bar{n}}}, \tag{A.3}$$

$$[K_{22}]_{m\bar{n}} = \left(A_s R + \frac{D_s}{R}\right)\left(\frac{n^2}{R^2} X^{00}_{\bar{n}m} C_n + \frac{1-v}{2} X^{11}_{\bar{n}m} S_n\right) + \sum_{k=1}^{N_r}\left[\left(\frac{d_r}{R} + \frac{S_r}{R^2}\right)\left\{n^2 A_r \Phi^{00}_{\bar{n}m} C_n + \frac{(1-v)D_r}{2} \Phi^{11}_{\bar{n}m} S_n\right\} + n^2 D_r\left(\frac{d_r}{R^3} - \frac{S_r}{R^4}\right)\Phi^{00}_{\bar{n}m} C_n\right], \tag{A.4}$$

$$[K_{c23}]_{m\bar{n}} = \frac{n}{R}\left[\left(A_s + \frac{n^2 D_s}{R^2}\right) X^{00}_{\bar{n}m} C_n + D_s\{v X^{02}_{\bar{n}m} C_n + (1-v) X^{11}_{\bar{n}m} S_n\}\right] + \sum_{k=1}^{N_r}\left[\left\{A_r\left(\frac{n d_r}{R} + \frac{n^3 S_r}{R^2}\right) + n^3 D_r\left(\frac{d_r}{R^3} - \frac{S_r}{R^4}\right)\right\}\Phi^{00}_{\bar{n}m} C_n + \frac{n(1-v)D_r}{2}\left(\frac{2d_r}{R} + \frac{S_r}{R^2}\right)\Phi^{11}_{\bar{n}m} S_n\right] \tag{A.5}$$

$$[K_{33}]_{m\bar{n}} = \left(A_s + \frac{n^4 D_s}{R^2}\right)\frac{X^{00}_{\bar{n}m} C_n}{R} + D_s R X^{22}_{\bar{n}m} C_n - \frac{2n^2 v D_s}{R}(X^{02}_{\bar{n}m} + X^{20}_{\bar{n}m}) C_n + \frac{2n^2(1-v)D_s}{R} X^{11}_{\bar{n}m} S_n + \sum_{k=1}^{N_r}\left\langle\left[A_r\left\{\frac{d_r}{R} - \frac{S_r}{R^2} + n^4\left(\frac{I_r}{R^3} - \frac{I'_r}{R^4}\right) + 2n^2\left(\frac{S_r}{R^2} - \frac{I_r}{R^3}\right)\right\} + n^4 D_r\left(\frac{d_r}{R^3} - \frac{S_r}{R^4}\right)\right]\Phi^{00}_{\bar{n}m} C_n + \frac{n^2(1-v)D_r}{2}\left[\frac{4d_r}{R} - \frac{3I_r}{R^3} - \frac{I'_r}{R^4}\right]\Phi^{11}_{\bar{n}m} S_n\right\rangle, \tag{A.6}$$

$$[M_{11}]_{m\bar{n}} = \rho h R C_n \frac{X^{11}_{\bar{n}m}}{\alpha_{\bar{n}}\alpha_m}, \tag{A.7}$$

$$[M_{22}]_{m\bar{n}} = \rho h R S_n X^{00}_{\bar{n}m} + \sum_{k=1}^{N_r} \rho b_r\left[R d_r + 3S_r + \frac{3I_r}{R} + \frac{I'_r}{R^2}\right]\Phi^{00}_{\bar{n}m} S_n, \tag{A.8}$$

$$[M_{23}]_{m\bar{n}} = \rho b_r n\left[S_r + \frac{2I_r}{R} + \frac{I'_r}{R^2}\right]\Phi^{00}_{\bar{n}m} S_n, \tag{A.9}$$

$$[M_{33}]_{m\bar{n}} = \rho h R X^{00}_{\bar{n}m} C_n + \sum_{k=1}^{N_r} \rho_r b_r\left[n^2\left(\frac{I_r}{R} + \frac{I'_r}{R^2}\right) S_n + (d_r R + S_r) C_n\right]\Phi^{00}_{\bar{n}m}, \tag{A.10}$$

where

$$X^{pq}_{\bar{n}m} = \int_0^L \frac{\mathrm{d}^{(p)}\psi_{\bar{n}}}{\mathrm{d}x^{(p)}} \frac{\mathrm{d}^{(q)}\psi_m}{\mathrm{d}x^{(q)}}\,\mathrm{d}x, \tag{A.11}$$

$$\Phi^{pq}_{\bar{n}m} = \int_x \delta(x - x^*) \frac{\mathrm{d}^{(p)}\psi_{\bar{n}}}{\mathrm{d}x^{(p)}} \frac{\mathrm{d}^{(q)}\psi_m}{\mathrm{d}x^{(q)}}\,\mathrm{d}x, \tag{A.12}$$

$$(S_r \;\; I_r \;\; I'_r) = \int_{h/2}^{d_r+h/2} (z \;\; z^2 \;\; z^3)\,\mathrm{d}z, \tag{A.13}$$

$$S_n = \int_0^{2\pi} \sin^2 n\theta\,\mathrm{d}\theta. \tag{A.14}$$

References

[1] H. Kondo, Axisymmetric vibration analysis of a circular cylindrical tank, *Bulletin of the Japan Society of Mechanical Engineers* 24 (1981) 215–221.

[2] N. Yamaki, J. Tani, T. Yamaji, Free vibration of a clamped–clamped circular cylindrical shell partially filled with fluid, *Journal of Sound and Vibration* 94 (1984) 531–550.

[3] R.K. Gupta, G.L. Hutchinson, Free vibration analysis of liquid storage tanks, *Journal of Sound and Vibration* 122 (1988) 491–506.

[4] M. Amabili, M.P. Paidoussis, A.A. Lakis, Vibrations of partially filled cylindrical tanks with ring-stiffeners and flexible bottom, *Journal of Sound and Vibration* 213 (1998) 259–299.

[5] A.A. Lakis, M. Sinno, Free vibration of axisymmetric and beam-like cylindrical shells, partially filled with liquid, *International Journal of Numerical Methods in Engineering* 33 (1992) 235–268.

[6] T. Balendra, K.K. Ang, P. Paramasivam, S.L. Lee, Free vibration analysis of cylindrical liquid storage tanks, *International Journal of Mechanical Sciences* 24 (1982) 47–59.

[7] P.B. Goncalves, N.R.S.S. Ramos, Free vibration analysis of cylindrical tanks partially filled with liquid, *Journal of Sound and Vibration* 195 (1996) 429–444.

[8] T. Mikami, J. Yoshimura, The collocation method for analyzing free vibration of shells of revolution with either internal or external fluids, *Computers and Structures* 44 (1992) 343–351.

[9] K.-H. Jeong, S.-C. Lee, Hydroelastic vibration of a liquid-filled circular cylindrical shell, *Computers and Structures* 66 (1998) 173–185.

[10] T. Mazuch, J. Horacek, J. Trnka, J. Vesely, Natural modes and frequencies of a thin clamped–free steel cylindrical storage tank, *Journal of Sound and Vibration* 193 (1996) 669–690.

[11] B. Yang, J. Zhou, Analysis of ring-stiffened cylindrical shells, *Journal of Applied Mechanics* 62 (1995) 1005–1014.

[12] Y.S. Lee, Y.W. Kim, Vibration analysis of rotating composite cylindrical shells with orthogonal stiffeners, *Computers and Structures* 69 (1998) 271–281.

[13] Y.S. Lee, Y.W. Kim, Effect of boundary conditions on natural frequencies for rotating composite cylindrical shells with orthogonal stiffeners, *Advances in Engineering Software* 30 (1999) 649–655.

[14] Y.W. Kim, Y.S. Lee, Transient analysis of ring-stiffened composite cylindrical shells with both edges clamped, *Journal of Sound and Vibration* 252 (2002) 1–17.

[15] R.K. Gupta, Sloshing in shallow cylindrical tanks, *Journal of Sound and Vibration* 180 (1995) 397–415.

[16] SASI, *ANSYS User Manual*, Swanson Analysis System Inc., Houston, TX, 2000.